Flow Prediction around an Oscillating NACA0012 Airfoil at Re = 1 000 000

Octavian FREDERICH[1], Ulf BUNGE[2], Charles MOCKETT[1] and Frank THIELE[1]

[1] *Berlin University of Technology, Institute of Fluid Mechanics and Engineering Acoustics, Müller-Breslau-Str. 8, 10623 Berlin,* `Octavian.Frederich@tu-berlin.de`
[2] *IVM Automotive Wolfsburg GmbH, Wolfsburger Landstr. 22, 38442 Wolfsburg*

Abstract. The maximum obtainable lift of a rotationally-oscillating airfoil is significantly higher than in the static or quasi-static case. The correct prediction of dynamic stall as the basis of the dynamically increased lift is essential to quantify the time-dependent load on the airfoil structure. This study applies unsteady RANS (URANS) and detached-eddy simulation (DES) with various turbulence models and parameter variations in order to capture the physics around an oscillating NACA0012 airfoil at a relatively high Reynolds number and to identify possible advantages and potential drawbacks of the given methods. The quality of the flow prediction is assessed primarily on the basis of integral force coefficients compared to experimental results, revealing the influence of resolution on maximum lift and the corresponding angle of incidence.

Key words: NACA0012, oscillating airfoil, dynamic stall, URANS, DES.

1. Introduction

Flows around rotationally-oscillating airfoils are characterised by two important physical phenomena. On the one hand a hysteresis develops in the curves of lift and drag vs. angle of attack and on the other hand the maximum lift is much higher than in the static or quasi-static case. Both effects are associated with unsteady flow separation, which is also referred to as "dynamic stall". A dynamically affected process occurs when the oscillatory frequency is significantly higher than the frequency of potential vortex shedding in the presence of high angles of attack. Such patterns appear in diverse engineering applications e.g. helicopter rotor blades, turbo-machinery and wind turbines.
The configuration investigated here is a NACA0012 airfoil that oscillates sinusoidally around the quarter chord line and mean incidence of 15° with an amplitude of 10° at Reynolds number $\mathrm{Re}_c = 10^6$. With the reduced frequency of the oscillatory movement $k_{osc} = \pi f_{osc} c/u_\infty = 0.1$ and the estimated Strouhal number for the vortex shedding (vsh) of a NACA0021 $\mathrm{St} = f_{vsh} c/u_\infty = 0.2$ [8], the ratio $f_{osc}/f_{vsh} \approx 18$ confirms the existence of a dynamically affected stall. This also reveals that the large-scale dynamics in the stalled flow are dominated by the prescribed motion of the airfoil in contrast to the vortex shedding behind a steady airfoil at high angle of attack or behind a bluff body.
The present case comprises an oscillation around the maximum lift, and thus the challenge to rise to is the massively-separated flow after stall and the accompanying

highly unsteady flow physics. The time-accurate prediction of this is essential to enable a correct prediction of any fluid-structure interaction. This has already been outlined in [3], where turbulence-resolving and more advanced simulation methods such as detached-eddy simulation (DES) are recommended. With integral values in the focal point of interest though, unsteady RANS (URANS) is in some cases seen to be sufficient in this study due to the aforementioned motion-induced unsteadiness of the flow. This will be demonstrated by comparison with experimental results averaged over 200 cycles that have been published by McAlister *et al.* [6].

2. Numerical Method and Parameters

The flow field around the NACA0012 airfoil is discretised using block-structured grids with varying topology and spatial resolution. Concerning the spatial discretisation, a c-type grid arranged for URANS boundary layer predictions with 35 000 cells in each 2D slice is tested against an o-type grid specially prepared for DES of massive separation with 46 000 cells in 2D. The spanwise domain size of one chord length is resolved for the c-type grid by 3, 11 and 21 nodes (variants C3, C11, C21), whereas the number of nodes for the o-type grids is 60. Two different o-type grids are considered (variants 01 and 02), which differ only in the wall-normal refinement of the boundary layer region. The 02 variant exhibits a fine resolution of $y^+ < 1$ throughout the oscillation cycle. A no-slip condition is applied to the physical wall with a universal hybrid treatment implemented to the turbulence equations allowing arbitrary values of y^+. A periodic condition is applied to the lateral boundaries and a convective outflow condition to the downstream boundary. The whole grid is rotated sinusoidally using rigid body motion, thus a constant inflow profile with the bulk velocity u_∞ is sufficient.

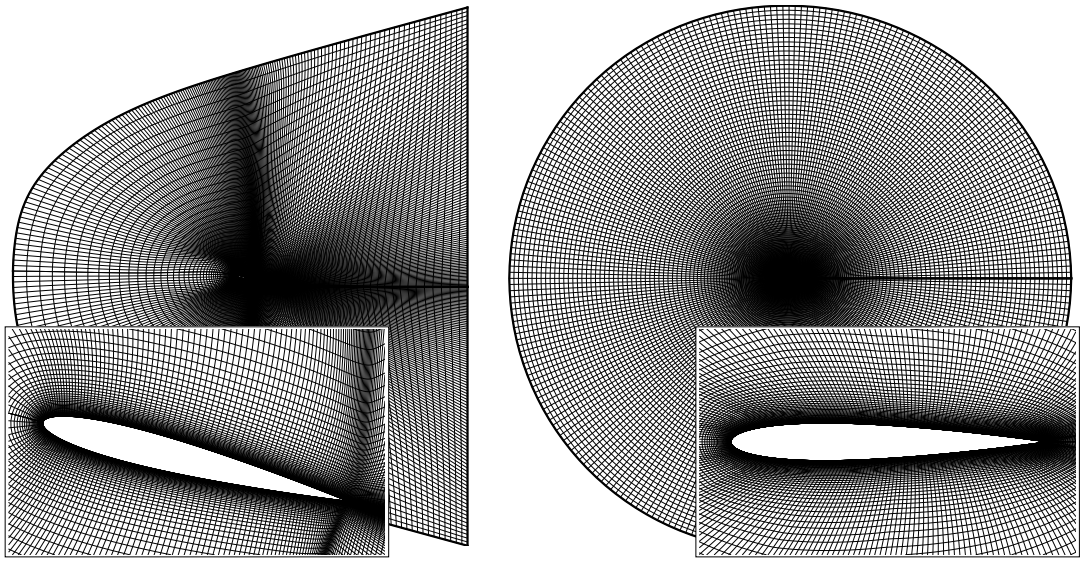

Figure 1. 2D planes of the c-type and o-type grids.

With focus on the integral force coefficients of relevance for engineers, URANS simulations were performed on the c-type grid and DES on all grid types. Turbulence models with varying degrees of complexity are used, such as the SALSA

one-equation [9], the two-equation LLR k-ω [10] and an explicit algebraic stress model, the CEASM [5]. For details the reader is referred to [1], where a detailed description of the implementation of these models and their DES variants is given. The investigations were performed using the solver ELAN developed at the Berlin University of Technology. This numerical procedure uses a conservative finite-volume discretisation based on general curvilinear coordinates of the Navier–Stokes equations for incompressible and compressible flows. The spatial discretisation of the diffusive and convective terms is realised using central differencing, and a backward difference quotient of first or second order accuracy is used for the temporal derivative [12]. The code has been enhanced towards DES as well as an arbitrary Lagrange-Eulerian formulation (ALE) to capture moving and deforming grids [2], and is therefore able to handle all common simulation approaches such as URANS, DES, LES as well as direct numerical simulation for a wide range of engineering applications. The correct treatment of moving grids is realised with the space conservation law which is important for the presented case. In order to prevent unwanted encroachment of the LES mode of the DES inside attached turbulent boundary layers, the delayed DES (DDES) shield function of Spalart *et al.* [7] has been implemented to the CEASM-based DES.

3. Flow Physics

For the configuration investigated, the airfoil exhibits a sinusoidal oscillation between 5° and 25°. Such harmonics around the maximum static lift are characterised by a forced rotatory movement of the wing or an equivalent unsteady inflow condition with viscous effects dominating the flow. The flow phenomena during the oscillation period and the pressure distribution on the central airfoil section predicted by a numerical simulation are visualised in figures 2 and 3.
By rapidly increasing the incidence of the airfoil beyond the static separation angle the boundary layer on the upper side of the profile becomes fully turbulent. When further increasing the incidence a vortex starts to develop at the separation of the turbulent boundary layer near the profile's leading edge. The vortex grows very fast and is convected downstream, while remaining close to the surface, increasing drastically the suction on the upper side. The maximum dynamic lift is created as the vortex is transported just beyond the streamwise midpoint of the profile, but before the maximum incidence is reached. The vortex suction is reduced further downstream until passing the trailing edge, thereby initiating full dynamic stall. The brief, wake-induced reattachment of the stalled region above the profile leads to an intermediate increase of the suction and the lift. Thereafter vortex shedding at the stalled airfoil occurs until the incidence has decreased such that the flow can reattach from the front to the rear.

4. Results

In the following, the results of the numerical simulations are summarised and evaluated with respect to the variation of individual parameters. The force coefficients obtained using the o-grids are phase-averaged with respect to the sinusoidal oscillation of the airfoil (section 4.5.). The analysis of the differences between two solutions is mainly focused on the numerical and modelling reasons for the deviation.

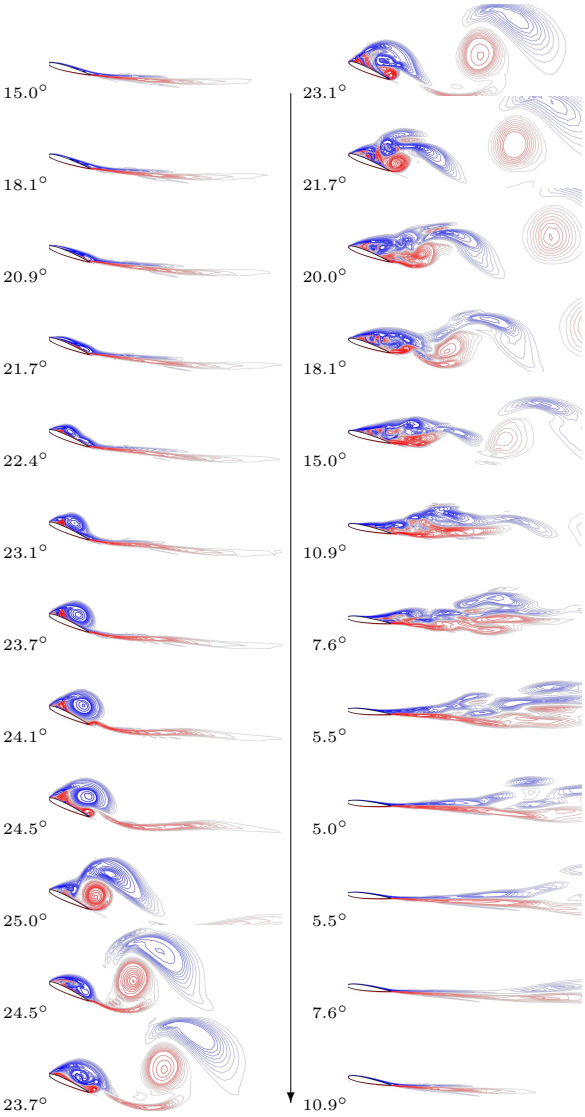

Figure 2. Instantaneous iso-lines of the z-vorticity (SALSA DES, O1, $\Delta t{=}T/300$)

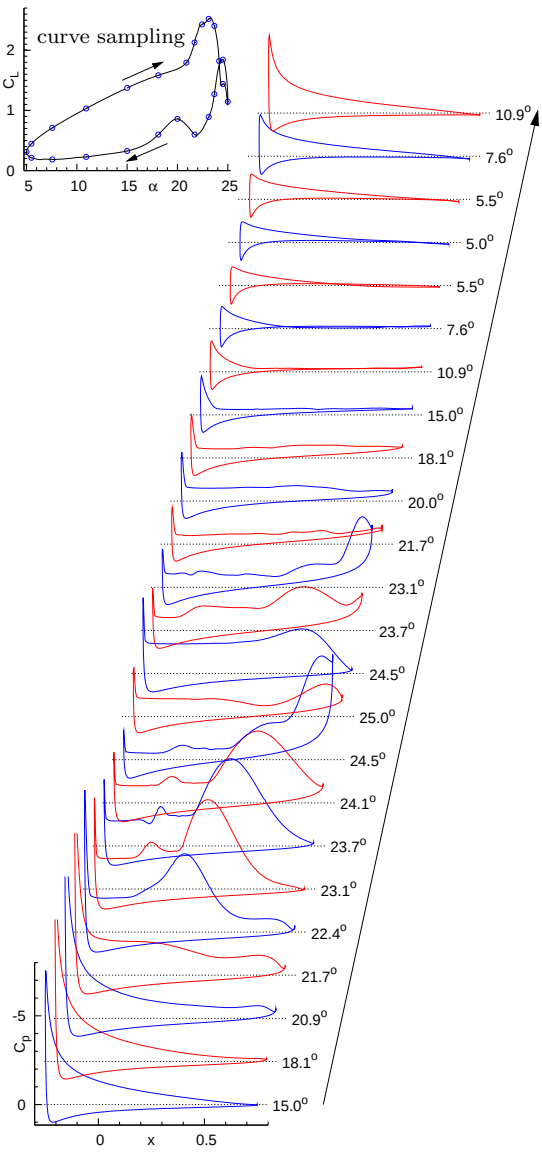

Figure 3. Instantaneous pressure coefficient C_p (SALSA DES, O1, $\Delta t{=}T/300$)

4.1. Spatial Resolution

The variation of the spatial resolution comprises two main parts. On the one hand there are two general grid topologies, and on the other hand the number of spanwise nodes is varied among the c-type grids as well as between c-type and o-type grids. The curves in figures 4 and 5 depict the lift coefficient predicted by URANS and DES with varying grids for different background models. Figure 4 clearly shows that for URANS the lift curve changes very slightly with increasing spanwise resolution (figure 4), whereas using DES the changes are significant, especially in the region of total stall. The flow predicted by URANS apparently tends to remain two-dimensional without considering the resolution of the span. The DES modification of the same equations results in a much reduced eddy viscosity through a length scale

based on the maximum grid dimension, i.e. the spanwise dimension in these highly under-resolved cases. Thus, the turbulent structures can more easily become three-dimensional, leading to a reduction of the secondary vortex shedding with increased spanwise resolution. This can be recognised in the lift curves of DES (figure 5) by the smoothing of the lift curve and the decreasing discrepancy compared to the experimental results.
The difference of the curves between c-type and o-type grids in figure 5 results from the fact that originally the c-type grid was adapted for boundary layer flows to be predicted by URANS, whereas the the o-type grid is as uniform as possible to account for the grid resolution necessary in the LES region. This fact, together with the improved agreement achieved by the c-type grid suggests that for this case capturing the dominant wall effects is essential for the integral force coefficients.
The convergence of the results with respect to the spanwise resolution is evident for URANS. In the case of DES clear convergence of the solution is not seen, but might be possible with further refined resolution of the span on the same grid topology.

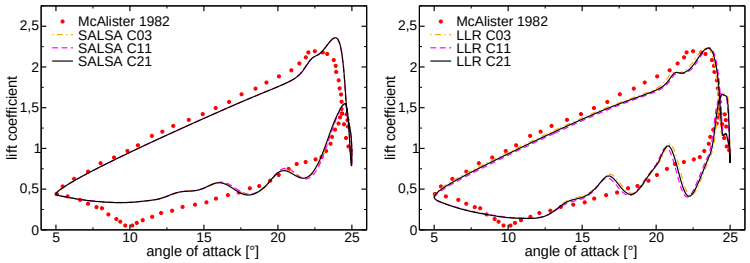

Figure 4. URANS: Lift coefficient with varying spatial resolution and $\Delta t{=}T/300$

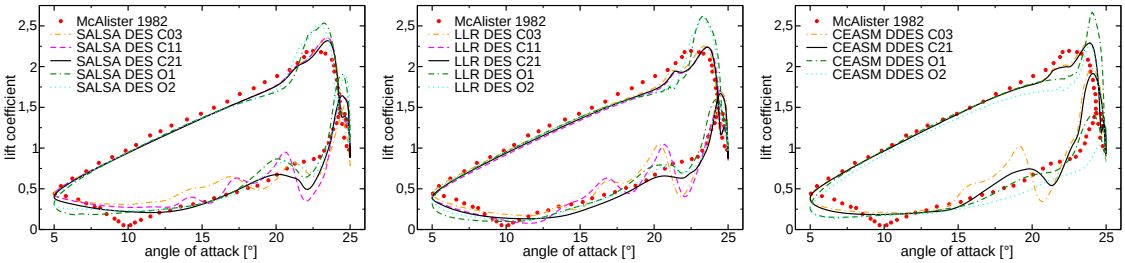

Figure 5. DES: Lift coefficient with varying spatial resolution and $\Delta t{=}T/300$

4.2. Temporal Resolution

The temporal discretisation is based on a varying number of 300, 600 and 1000 timesteps Δt to resolve a single period of oscillation $T_{osc} = \pi c/(k_{osc}u_\infty)$. The influence of the timestep size is investigated using the c-type grid with the coarsest spanwise resolution C03. This has been used to keep the required simulation expense within affordable limits.
The figures 6 and 7 show the lift curves for URANS and DES for fixed grid and background model. The results of the URANS simulations with the SALSA model clearly demonstrate convergence of the lift curve with refined temporal resolution. The same level of convergence can be recognised also for the SALSA DES as the timestep size is reduced. By contrast, the LLR k-ω is far from demonstrating convergence with increasing temporal resolution, neither for URANS nor DES. It is

evident that the simulation resolves more unsteadiness with reduced timestep size, but in case of the LLR k-ω model the numerical results increasingly deviate from the experimental results in the detached flow region predicting an excessive secondary vortex shedding that appears to be unphysical. The temporal dependency for the CEASM cannot yet be concluded from the results available.

The hypothesis that remains to be proven is that the LLR model constants have been derived based on the presence of excessive numerical dissipation (either from coarse grids or overly-dissipative numerical schemes), giving rise to a model that itself is insufficiently dissipative. A RANS model should show independence of the time step beyond a certain extent, as the Reynolds-averaged paradigm upon which it is derived dictates that fine turbulent structures remain modelled using eddy viscosity irrespective of spatial and temporal resolution. It is supposed however that the LLR model does not produce sufficient eddy viscosity to damp small scale structures when the time filtering effect of a large numerical timestep is reduced, resulting in the unphysical "resolution" of fine-grained structures corresponding neither to a RANS or an LES.

Independent of the modelling approach used, the lift curves in figure 6 and 7 clearly show that the maximum lift and the corresponding angle of attack are reduced with increasing temporal resolution, which corresponds to better corroboration with the experimental results.

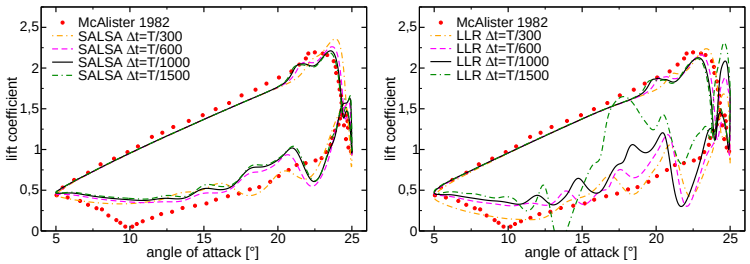

Figure 6. URANS: Lift coefficient with varying temporal resolution on C03-grid

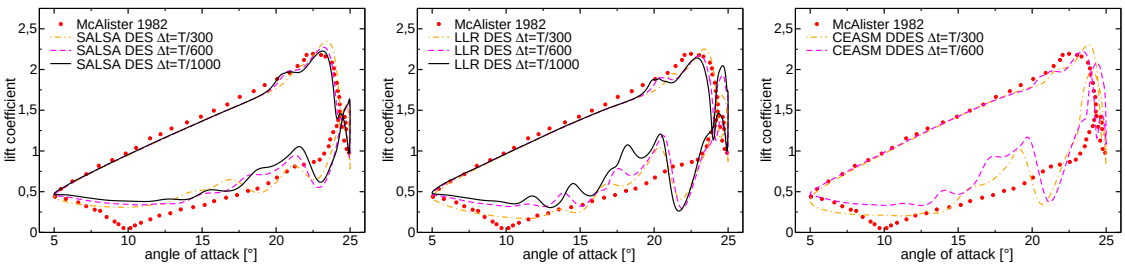

Figure 7. DES: Lift coefficient with varying temporal resolution on C03-grid

The curves in figures 6 and 7 reveal that the dynamics of the flow is already captured correctly for the extensively used timestep size of $\Delta t = T/300$. Although the Courant-Friedrichs-Lewy criterion $\mathrm{CFL} = u\Delta t/\Delta x \leq 1$ is not met overall for this temporal resolution, the influence on the flow prediction is relatively small and has been neglected in order to achieve a wider range of parameter variations with available computational resources.

4.3. URANS versus DES

In the figures 8 and 9 the lift and drag curves are shown such that the model influence can be judged on a fixed grid. In the case of URANS, figure 8, the results demonstrate that the solution does not depend on the spatial resolution but on the turbulence model used. In addition, comparison to the experimental results reveals that the LLR k-ω model agrees slightly better with these.
In contrast to URANS, the results obtained using DES show on the one hand a significant dependency upon the spanwise resolution, and on the other a reduced dependency on the turbulence model used. This behaviour arises from the hybrid synthesis of RANS and LES, where the LES activity and RANS/LES blending location causes the differences in the results for varying spatial resolution and the RANS region is mainly responsible for the model influence, visible in figure 9.

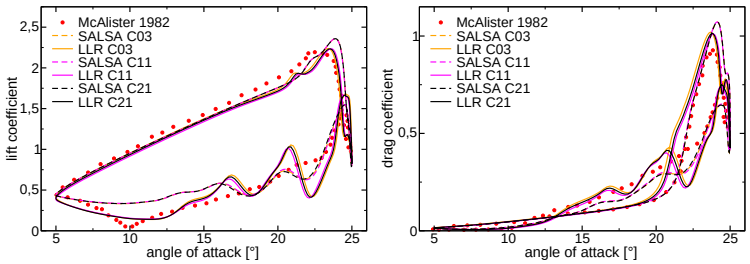

Figure 8. Lift and drag coefficient for URANS on fixed grid and $\Delta t{=}T/300$

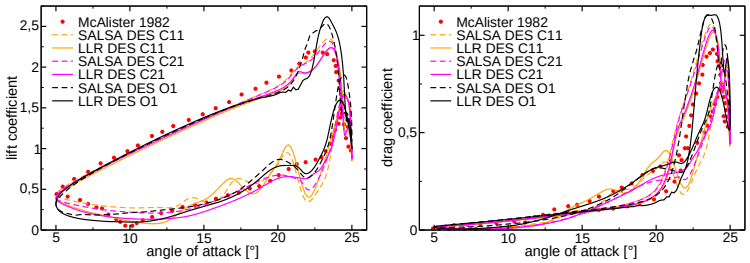

Figure 9. Lift and drag coefficient for DES on fixed grid and $\Delta t{=}T/300$

4.4. Model Influence

For the present configuration the maximum lift is experienced before the maximum incidence is reached. This behaviour is predicted by all models and for all grids (see figures 10, 11). However, the angle of attack where the dynamic stall occurs is predicted best by the one-equation SALSA model compared to the two-equation models, even though the angle on the c-type grid and the maximum lift on the o-type grid are predicted too highly. The latter aspects can also be observed for the LLR k-ω model but with slightly degraded performance concerning the prediction of the maximum lift and the associated incidence. Nevertheless the agreement of the results for this model with the experimental results is somewhat better close to the maximum incidence, where secondary vortex shedding occurs.
The $k-\varepsilon$-based CEASM has only been applied in the DDES variant and URANS has not yet been performed with this model. The force coefficients obtained for this model on the C21-grid, shown in figure 11, reveal the changing quality of the pre and post-stall prediction. On the one hand the predicted lift matches the experimental

results during the upstroke until the dynamic stall vortex develops, whereas on the other hand the discrepancy with the experiments is much higher than for the other models, especially noticeable in the drag curve. The results obtained on the O2-grid show the opposite behaviour for the lift and drag; the drag agrees well with the experimental results in the pre-stall period, whereas the lift curve and the post-stall part of the drag are poorly predicted.
Taking into account that the c-type grid resolution is focused close to the profile and for the o-type grid a uniform resolution in the wake was preferred, the conclusion is that capturing the physics near the profile is essential for the size of the maximum lift and the sufficient wake resolution is the basis for the correct dynamic stall angle. This thesis is supported by the results of the SALSA and LLR models, and partly those of the CEASM model.

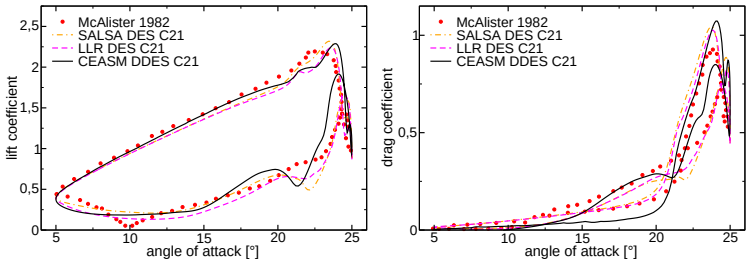

Figure 10. Lift and drag coefficient with varying DES background model (C21, $\Delta t{=}T/300$)

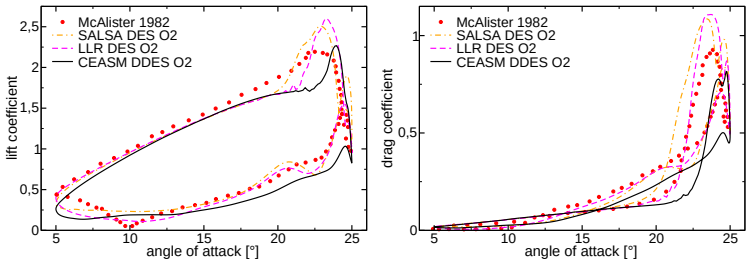

Figure 11. Lift and drag coefficient with varying DES background model (O2, $\Delta t{=}T/300$)

4.5. Numerical Aspects

The DES approach is a hybrid of RANS and LES. To obtain stable but also physical solutions for a given problem, it has been ensured that for both modes the favourable convection scheme will be used - in case of RANS upwind-based and for LES central schemes. Thus, the DES modification of the turbulence equations is connected with the usage of a hybrid convection scheme [11]. The blending of upwind-based and central schemes depends mainly on the local flow solution and is therefore not limited to DES.
The importance of the hybrid convection scheme is demonstrated by the lift curves in figure 12. Depicted are URANS solutions obtained with an upwind-based TVD scheme, with the hybrid scheme and the respective DES solution. In case of the SALSA model, it is evident that the main improvement of DES relative to URANS is based on the convection scheme (at least for this relatively coarse grid). For the LLR k-ω a small improvement can also be recognised in the downstroke region. This comparison reveals that URANS flow predictions can be improved by adapted numerical schemes, especially in the presence of flow separation.

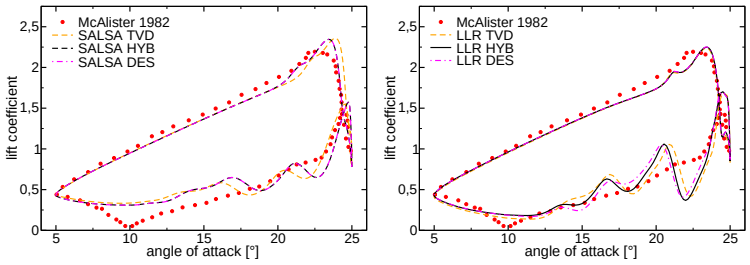

Figure 12. Lift coefficient with varying convection scheme or DES (C03, $\Delta t{=}T/300$)

Starting a testcase from scratch, the temporal behaviour of the flow solution passes several periodic cycles (2–4) until initial perturbations are decayed. As can be recognised in figure 13, the solution reaches a stable periodic state represented by the nearly perfect reproduction of the lift curve in successive cycles for the coarse C03-grid. With increasing spatial resolution of the span, the convergence of the hysteresis is reduced to the upstroke phase of the airfoil. Due to the variations in this phase for fine spanwise resolution, the integral quantities obtained for the o-grids are phase-averaged with respect to the oscillation of the airfoil. However, the consistent reproduction of the lift curve with minor variations for an arbitrary number of cycles is caused by the entire reattachment of the flow without vortex shedding at the minimum incidence, and assisted by the timestep size chosen as an exact partition ratio of the periodic time. Thus, the hysteresis converges also for such – relative to the averaged experimental data – seemingly unphysical results predicted by the LLR k-ω at fine temporal resolution.

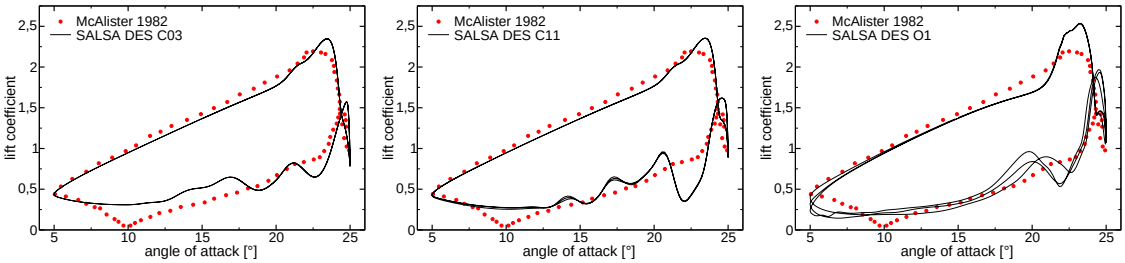

Figure 13. Lift coefficient in 3 successive cycles on varying grid (SALSA, $\Delta t{=}T/300$)

5. Conclusion and Outlook

Numerical simulations using URANS and DES were performed for the flow around an oscillating NACA0012 airfoil in order to identify important parameters influencing the prediction of the dynamic load on the structure. Both approaches can be used to capture the dynamics of the dynamic stall phenomenon correctly with acceptable discrepancies to few experimental results, but with some restrictions according mainly to the spatio-temporal resolution. Moreover, the necessity of sufficient spatial resolution in the spanwise direction as well as a very good circumferential resolution and in the wake has been clearly demonstrated. In addition, the prediction of the stall angle and the maximum lift is improved with increased temporal resolution.

The results reveal that the one-equation SALSA model seems to be more robust and captures most of the physics for this case than the two-equation models applied.

The technology feedback from DES to URANS, namely the application of a hybrid convection scheme for URANS, can improve the flow prediction without additional resolution.
The ongoing work and further research will concentrate especially on the refinement in time and space. Therefore, the circumferential node distribution in the O-type grid will be improved and c-type grids with increased spanwise resolution, e.g. C41 and C61, will be used. In this context, the impact of an increased spanwidth, refined temporal resolution (such that CFL ≤ 1 is achieved) as well as the hybrid convection scheme applied to URANS on a fine grid will be investigated. To side-step the problems experienced with the two-equation models, more established standard models such as the Wilcox k-ω, will be considered. The hypothesis concerning the possible recalibration of the LLR k-ω model should be further investigated, which would certainly require more comprehensive experimental results and additional testcases.

Acknowledgements

The support of the EU within the DESider project (Detached Eddy Simulation for Industrial Aerodynamics – `http://cfd.me.umist.ac.uk/desider`), contract-no. AST3-CT-200-502842 and the IBM pSeries 690 of the North German cooperation for High-Performance Computing (HLRN) facility is gratefully acknowledged.

References

[1] Bunge, U., Mockett, C., Thiele, F. (2007) *Guidelines for implementing Detached-Eddy Simulation using different models.* Aerospace Science and Technology, in press, online available, doi:10.1016/j.ast.2007.02.001.

[2] Bunge, U. (2004) *Numerische Simulation turbulenter Strömungen im Kontext der Wechselwirkung zwischen Fluid und Struktur.* PhD thesis, ISTA, TU Berlin.

[3] Bunge, U., Gurr, A., Thiele, F. (2003) *Numerical aspects of simulating the flow–induced oscillations of a rectangular bluff body.* Journal of Fluids and Structures **18**(3-4), 405–424.

[4] Frederich, O. (2003) *Numerical simulation of oscillating airfoils in turbulent flow with URANS and DES in comparison.* Diploma thesis, ISTA, TU Berlin.

[5] Lübcke, H. (2001) *Entwicklung expliziter Darstellungen zweiter statistischer Momente zur numerischen Simulation turbulenter Strömungen.* PhD thesis, ISTA, TU Berlin.

[6] McAlister, K.W., Pucci, S.L., Carr, L.W. and McCroskey, W.J. (1982) *An experimental study of dynamic stall on advanced airfoil sections.* NASA TM-84245.

[7] Spalart, P., Deck, S., Shur, M., Squires, K., Strelets, M., & Travin, A. (2006) *A new version of detached-eddy simulation, resistant to ambiguous grid densities.* Theoretical and Computational Fluid Dynamics, 20:181–195.

[8] Swalwell, K.E., Sheridan, J. & Melbourne, W.H. (2003) *Frequency analysis of surface pressure on an airfoil after stall.* 21. AIAA Applied Aerodynamics Conference.

[9] Rung, T., Bunge, U., Schatz, M. & Thiele, F. (2003) *Restatement of the Spalart–Allmaras Eddy–Viscosity Model in Strain–Adaptive Formulation.* AIAA Journal **41**(7), 1396–1399.

[10] Rung, T. & Thiele, F. (1996) *Computational Modelling of Complex Boundary–Layer Flows.* Proc. 9th Int. Symp. on Transport Phenomena in Thermal-Fluid Eng., Singapore, 321–326.

[11] Travin, A., Shur, M., Strelets, M. & Spalart, P. (2000) *Physical and Numerical Upgrades in the Detached-Eddy Simulation of Complex Turbulent Flows.* Proc. of the 412th Euromech Colloquium on LES and Complex Transitional and Turbulent Flows, Munich.

[12] Xue, L. (1998) *Development of an efficient parallel solution algorithm for the three-dimensional simulation of complex turbulent flows.* PhD thesis, ISTA, TU Berlin.